J. Astrophys. Astr. (2022) 43:9
https://doi.org/10.1007/s12036-021-09793-5

ACTIVE GALACTIC NUCLEI

Optical flux and spectral characterization of the blazar PG 1553 + 113 based on the past 15 years of data

ADITI AGARWAL[1,*], B. MIHOV[2], I. ANDRUCHOW[3,4], SERGIO A. CELLONE[4,5], G. C. ANUPAMA[6], V. AGRAWAL[7], S. ZOLA[8,9], AYKUT ÖZDÖNMEZ[10] and ERGÜN EGE[11]

[1]Raman Research Institute, C. V. Raman Avenue, Sadashivanagar, Bengaluru 560080, India.
[2]Institute of Astronomy and NAO, Bulgarian Academy of Sciences, 72 Tsarigradsko Chaussee, Blvd., 1784 Sofia, Bulgaria.
[3]Instituto de Astrofísica de La Plata (CCT La Plata-CONICET-UNLP), La Plata, Argentina.
[4]Facultad de Ciencias Astronómicas y Geofísicas, Universidad Nacional de La Plata, Paseo del Bosque, B1900FWA La Plata, Argentina.
[5]Complejo Astronómico "El Leoncito" (CASLEO), CONICET-UNLP-UNC-UNSJ, San Juan, Argentina.
[6]Indian Institute of Astrophysics, Block II, Koramangala, Bangalore 560034, India.
[7]Twilio, RMZ Ecoworld, Bellandur, Bangalore 560103, India.
[8]Astronomical Observatory, Jagiellonian University, ul. Orla 171, 30-244 Krakow, Poland.
[9]Mt. Suhora Observatory, Pedagogical University, ul. Podchorazych 2, 30-084 Krakow, Poland.
[10]Department of Astronomy and Space Science, Faculty of Science, Ataturk University, Yakutiye, Erzurum, Turkey.
[11]Department of Astronomy and Space Sciences, Faculty of Science, Istanbul University, 34116 Beyazıt, Istanbul, Turkey.
*Corresponding author. E-mail: aditi.agarwal@rri.res.in

MS received 10 August 2021; accepted 3 November 2021

Abstract. We study flux and spectral variability of the high energy peaked TeV blazar PG 1553 + 113 on diverse timescales using the data collected from 2005 to 2019 which also includes the intensive intra-night monitoring of the target. Additionally, we recorded the brightest flare of the blazar PG 1553 + 113 during April 2019 when the source attained an *R*-band magnitude of 13.2. Analyzing the spectral evolution of the source during the flare gave a clockwise spectral hysteresis loop and a time lag with *V*-band variations leading to the *R*-band ones. Various statistical tests, fitting procedures and cross-correlation techniques are applied to search for periodicity and examine the color-magnitude relationship. We find a median period of (2.21 ± 0.04) years along with the secondary period of about 210 days. Finally, we briefly discuss various physical mechanisms which are capable of explaining our findings.

Keywords. Active galaxies—BL Lacertae objects—PG 1553 + 113.

1. Introduction

Blazars are an extreme class of active galactic nuclei (AGN) characterized by large flux density and polarization variability on diverse timescales and across the entire electromagnetic (EM) spectra. Blazar family consists of BL Lacertae (BL Lac) objects and flat-spectrum radio quasars (FSRQs) depending on the characteristics of their broad emission lines; the former have strong emission lines in their optical spectra while the latter have very weak or no such lines (Urry & Padovani 1995). Broadband spectral energy distribution (SED) of a blazar display two hump structure. The first one peaks between the IR and X-ray energies and can be attributed to synchrotron emission of relativistic electrons. The other component peaks in the MeV to TeV energy range. Within the leptonic scenarios, the

This article is part of the Special Issue on "Astrophysical Jets and Observational Facilities: A National Perspective".

Published online: 15 February 2022

second component can be attributed to inverse-Compton emission of the seed photons produced locally (synchrotron self-Compton; SSC), or the external photons (external Compton; EC) from the accretion disk, the broad-line region (BLR), or the dusty torus (DT). Alternatively, in hadronic scenarios, the second peak is believed to be due to hadronic and lepto-hadronic processes (Böttcher *et al*. 2013; Cerruti 2020).

Blazar variability can be detected on diverse timescales and is conventionally divided into intra-night/day variability (INV/IDV; also commonly called microvariability) with variations on timescales from minutes to hours, short-term variability (STV) with variations from months to weeks and long-term variations ranging from months to years (Wagner & Witzel 1995; Gupta *et al*. 2008a; Agarwal *et al*. 2017; and references therein). Variability is a powerful tool to understand the nature of blazar and the dominant emission processes (Bhatta & Webb 2018).

The blazar PG 1553 + 113, first discovered by the Palomar-Green survey of UV-excess stellar objects (Green *et al.* 1986) is classified as a BL Lac object due to the absence of broad emission lines in its optical spectrum. Due to its featureless optical spectrum and non-detection of the host galaxy, its redshift remains uncertain. The recent studies of its putative galaxy group would set its redshift at $z = 0.433$ (Johnson *et al.* 2019). PG 1553 + 113 is significantly variable and well-observed at all frequencies from radio to gamma-rays. It has been one of the targets of various recent multiwavelength observing campaigns, some of which included studying its highly variable nature. Furthermore, it has been classified as an HBL, as its synchrotron emission peak falls in the UV and X-ray frequency range (Falomo & Treves 1990).

In the past decade, many studies have been dedicated to QPO search in AGNs thus motivating us to explore it further through this work. Quantifying QPOs in AGNs will further enable us to constrain theoretical models available in literature such as the orbiting hot spot on AD (Mangalam & Wiita 1993), turbulence behind shock in the Doppler boosted jet (Camenzind & Krockenberger 1992) and the swinging jet model (Gopal-Krishna & Wiita 1992).

Along with flux variability studies, search for the presence of quasi-periodicities in blazar light curves and spectra have begun to be implemented in the last decade. Quasi-periodicity in blazars is a controversial issue because of its relation to the possible binary systems of supermassive black holes (SMBHs). PG 1553 + 113 is one of the few blazars whose flux variations are claimed to be periodic (Ackermann *et al.* 2015, Tavani *et al.* 2018; Covino *et al.* 2020 and references therein). On the other hand, Covino (2019) and Ait Benkhali *et al.* (2020) expressed some caution about the significance of the year-long period detected at γ-rays. Nilsson *et al.* (2018) and Lico *et al.* (2020) did not find the claimed periodic variability in the *R*-band and radio LCs of the source, respectively.

The paper is organized as follows: the observations and data reduction methods are described in Section 2. We report the results of flux, color and spectral variability of the source from intra-night to longer timescales in Section 3, finally, Section 4 presents a discussion and conclusion based on our results.

2. Observations and data reduction

We observed the source for a total of 76 nights from January 2016 to August 2019 in the optical *BVRI*-bands using nine different telescopes around the globe, which are: 2.15 m Jorge Sahade telescope (JS, telescope A) and 60 cm Helen Sawyer Hogg telescope (HSH, telescope B), CASLEO, Argentina; 2.0 m Ritchey–Chrétien (RC, telescope C) and 50/70 cm Schmidt (telescope D) at the Rozhen National Astronomical Observatory (NAO), Bulgaria; 2.01 m RC Himalayan Chandra telescope (HCT, telescope E) at Indian Astronomical Observatory, Hanle, India; 1.3 m JC Bhattacharya telescope (JCBT; telescope F) at the Vainu Bappu Observatory (VBO), India; 1.0 m RC telescope (telescope G) and 60 cm RC robotic telescope (telescope H) at TUBITAK National Observatory (TUG), Antalya, Turkey; 50 cm Cassegrain telescope (telescope I) located at the Astronomical Observatory of the Jagiellonian University in Krakow, Poland.

The technical details for telescopes A, B, C, D and E can be found in Table 1 of Agarwal *et al.* (2019). The four other optical telescopes (F, G, H, I) are briefly described below.

The JCBT telescope located at the VBO, Tamil Nadu, India, is equipped with a 1k × 1k proEM CCD and a 2k × 4k regular CCD. The proEM CCD has a smaller field of view and to perform differential photometry, we need suitable pairs of non-variable stars from the same frame. Therefore, we used the 2k × 4k CCD to observe our source. The 1.0 m RC telescope located at the Bakirlitepe Mountain and currently operated remotely from TUG in Antalya is equipped with 4k × 4k CCD (working at −90°C) and has *BVRI* filters.

Table 1. Long-term variability characteristics.

Passband (1)	Weighted mean magnitude (2)	Faintest magnitude (3)	JD (4)	Brightest magnitude (5)	JD (6)	A [mag] (7)
B	14.501 ± 0.027	15.172	2457400.66179	13.893	2458588.36564	1.151
V	14.156 ± 0.026	14.646	2457612.30060	13.511	2458588.36235	1.135
R	13.790 ± 0.024	14.444	2457400.65818	13.212	2458588.35905	1.116
I	13.240 ± 0.028	13.970	2457400.66539	12.768	2458588.36099	1.071

Table columns read: (1) passband of observation, (2) weighted mean magnitude, (3) faintest magnitude attained by the source, (4) JD corresponding to the faintest magnitude, (5) brightest magnitude attained by the source, (6) JD corresponding to the brightest magnitude and (7) variability amplitude expressed in magnitudes instead of percents (see Equation (4) in Agarwal *et al.* 2019).

The 60 cm RC robotic telescope also located at TUG is equipped with a 2k × 2k CCD camera and 12 standard filters. The observations were done daily with 1k × 1k binning and 1–2 sets of *BVRI* frames.

Another telescope used is the 50 cm Cassegrain telescope located at the Astronomical Observatory of the Jagiellonian University in Krakow, Poland which is equipped with an Apogee Alta U42 CCD and a set of broadband filters. The source was observed in *BVRI* data with 2 × 2 binning and exposure between 60 s and 100 s. This camera accommodates an e2v, back-illuminated chip with 2048 px of 13 μm in size.

A detailed description of the data reduction procedure can be found in Agarwal & Gupta (2015). The calibration of instrumental magnitudes was made using magnitudes listed in Raiteri *et al.* (2015). In the course of this monitoring campaign, we acquired a total of ∼3350 data points in *BVRI*-bands.

In addition to the above data sets, we also used some of the major public data sets listed below. The Steward Observatory[1] of the University of Arizona observed the source in the *VR* filters from 2012 to 2018 (Smith *et al.* 2015); another major *VR* data set comes from Itoh *et al.* (2016) where authors performed the observations of the source from 2008 to 2014 using the Kanata telescope; Catalina Surveys performed observations (Drake *et al.* 2009) without a filter during 2005–2014 and the photometry has been transformed by the Catalina pipeline to *V*-band;[2] All-Sky Automated Survey for Supernovae[3] have observations from 2013 to 2018 in *V*-band (Jayasinghe *et al.* 2019). The Zwicky Transient Facility[4] – the data time span is from 2018 to 2019 and the *gr* magnitudes were transformed to the Johnson–Cousins *VR* ones (Masci *et al.* 2019); Katzman Automatic Imaging Telescope[5] – the unfiltered magnitudes roughly correspond to the *R*-band Filippenko *et al.* (2001), when checked on the basis of 34 nights in common; Observations from Tuorla Blazar Monitoring Program[6] were taken from 2005 to 2012 in the *R*-band (Takalo *et al.* 2008); Intermediate Palomar Transient Factory[7] – source monitored from 2009 to 2010 in *R* passband (Rau *et al.* 2009).

The so assembled *VR* LCs for the blazar PG 1553 + 113 are presented in Figure 1.

3. Results

Using those LCs which had a minimum of 10 data points in a single night, we studied IDV properties of the blazar PG 1553 + 113 during a total of 28 nights. Considering the modest number of points in a single filter, we used the *C*-test and the *F*-test, to assign variability status to the intra-night LCs (Agarwal *et al.* 2019). The LC is marked as variable if both tests rejected the null hypothesis at a 99.5% confidence level and non-variable (NV) if one of the tests failed to reject the null hypothesis. We did not find any significant variability during 28 nights thus resulting in a zero duty cycle.

Our long-term *BVRI*-band LCs are presented in Figure 1. Both statistical tests when applied to our long-term LCs revealed a significant variability at all four photometric passbands.

The most remarkable feature of our source is the brightest ever flare that was detected in all filters on 14

[1] http://james.as.arizona.edu/∼psmith/Fermi/.

[2] http://nesssi.cacr.caltech.edu/DataRelease/FAQ2.html.

[3] http://www.astronomy.ohio-state.edu/asassn/index.shtml.

[4] https://www.ztf.caltech.edu/.

[5] http://herculesii.astro.berkeley.edu/kait/agn/.

[6] http://users.utu.fi/kani/1m/.

[7] https://www.ptf.caltech.edu/iptf.

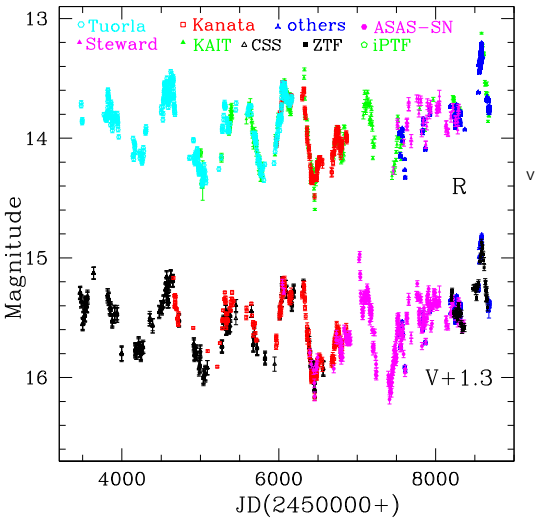

Figure 1. Long-term *VR*-band LCs for PG 1553 + 113. Different colors and symbols denote data from different telescopes as given in the plot. In particular, 'others' denote the data collected by the nine telescopes mentioned in Section 2.

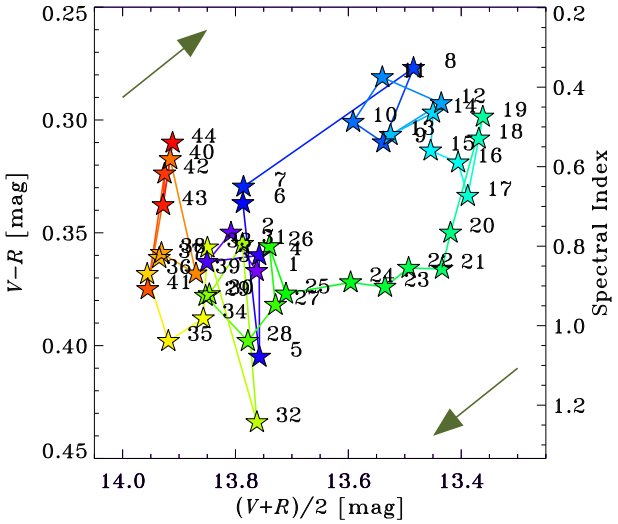

Figure 2. Color-magnitude diagram for the 2019 flare. The spectral index is also given: $\alpha \propto [(V-R)-(A_V-A_R)-0.186]/0.07$ where A_V and A_R stand for the Galactic extinction in the *VR*-bands, respectively. The colors and numbers are sequential in time: violet (#1) → red (#44) and arrows guide us through the loop directions.

April 2019 reaching the highest *R* flux level of 13.212 mag.[8] Whereas, the blazar reached the faintest state on 12 January 2016 with an *R* magnitude of 14.444. We also observed a larger variability amplitude at higher frequencies trend every year. The LTV characteristics are displayed in Table 1.

Multiband optical flux changes are accompanied by spectral changes. Coordinated optical multi-wavelength campaigns prove to be highly beneficial in studying color-magnitude behavior which could shed some light on the physical processes behind the blazar flux and spectral variations. In this context, we calculated color indices by coupling multi-band observations taken during the same night.

To inspect the flux and color index behavior, we divided the LCs into separate segments. As is evident from the Figure 1 one can see 5 distinct minima that divide the LCs and thus can be divided into 6 flares. Moreover, the 6th one can be divided as a pre-flare (around MJD of 8000) and a flare thus giving us a total of seven segments. CM relationship was found to be most significant for the brightest April flare ($r_{\rm CMD} = 0.49$ and $p = 0.0007$). The remaining segments show either achromatism or non-significant chromatism.

The detailed study of the color (or spectral) index – magnitude relationship of the flare revealed a lag. The spectrum got its hardest value (point #8 in Figure 2) before the source attained the maxima (#19) and then softened till the flare ends. The corresponding CMD shows a clockwise hysteresis loop – the spectrum gets flatter (≡ BWB chromatism) as the flux increases and steepens (≡ RWB chromatism) as the flux decreases (Figure 2). Such hysteresis pattern is usually seen in HBLs at X-ray frequencies (Takahashi *et al.* 1996) and hints towards the presence of a time lag, $\mathcal{T}$. To search the presence of time lag we applied the discrete correlation function (DCF; Figure 3) first introduced by Edelson & Krolik (1988) and the *z*-transformed DCF (ZDCF, Figure 3) (Alexander 1997) on the *V*- and *R*-band LCs and the time lag was determined by the Gaussian fitting and the centroiding methods. We found $\mathcal{T}_{\rm gauss} = (5.76 \pm 1.48)$ days using the Gaussian fit and $\mathcal{T}_{\rm cent} = 3.71$ days using the weighted centroid. The DCF is shown in Figure 3.

We then searched for the quasi-periodicity in PG 1553 + 113 by fitting sine function of the form $F(t) \propto \sin(2\pi t/P + \Phi)$ (P and Φ denote the period and phase, respectively). We detected periods of (807 ± 20) days and (812 ± 30) days for the *V*- and *R*-band LCs, respectively.

We also applied the classical Lomb–Scargle periodogram (LSP) method (Lomb 1976). The most significant peaks correspond to periods of (803 ± 70) days and (801 ± 62) days, for the *V*- and *R*-band LCs, respectively. These periods agree (within error) with those obtained from the sine fits. To test the significance of the peaks against the red noise background,

[8] http://www.astronomerstelegram.org/?read=12695.

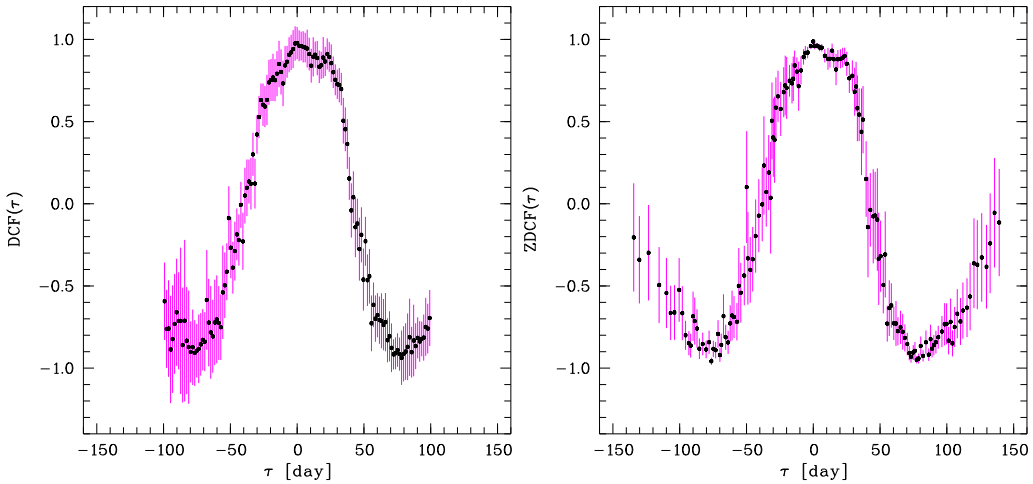

Figure 3. The leftmost figure displays the discrete correlation function of the source while the right one shows the ZDCF.

we utilized the REDFIT program (Ait Benkhali *et al.* 2020). The peaks exceeding the 99% significance level are at (772 ± 85) days and (817 ± 107) days, for the *V*- and *R*-band, respectively. The periods agree with the above estimates.

To further understand spectral variations in PG 1553 + 113, we generated its spectral energy distributions (SEDs) for considering all dates with quasi-simultaneous observations in at least three passbands. To display the changes in the SEDs of the source, we selected different states of the source as follows: an outburst state (13 March and 4 April 2019), intermediate state (11 June 2016, 10 May 2018 and 28 February 2019) and low state (12 January and 11 August 2016). These different SEDs (Figure 4) depict an increasing trend, thus indicating the fact that the synchrotron peak is located above 10^{15} Hz and thus is in accordance with the HBL classification. Therefore, from our optical study, we can conclude that the source behaves more like an HBL rather than an LBL. However, these SEDs cover a narrow wavelength range, therefore, further multi-wavelength analysis are in process to get a better diagnosis of its true class. To get the mean spectral index, we fitted the SEDs with a straight line of the form $\log(F_\nu) = -\alpha \log(\nu) + \text{const}$. We got $\alpha = 0.89 \pm 0.06$ with $\chi^2_{\rm df} = 1.1$, which are consistent with Falomo *et al.* (1994) and Pandey *et al.* (2019).

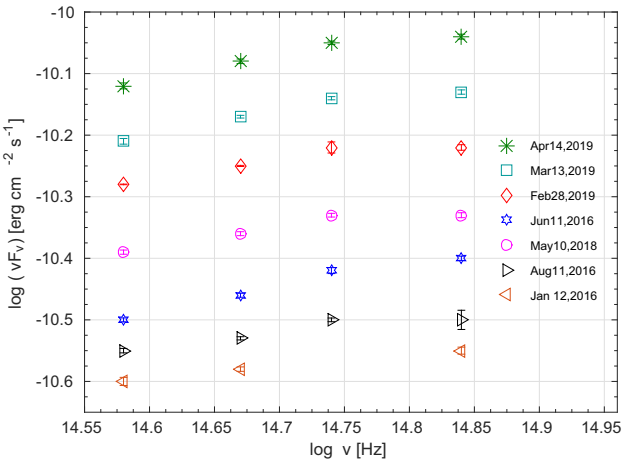

Figure 4. Optical SEDs of PG 1553 + 113 for different flux states as described in the text.

4. Discussion and conclusions

In this article, we have studied the multiband flux and spectral variability of the blazar PG 1553 + 113 on diverse timescales and searched for the presence of any quasi-periodicities. During the analyzed period from 2005 to 2019, we recorded in the brightest state of the source in April 2019 with an R band magnitude of ≃13.2. We found no significant variability during 28 IDV nights thus giving a zero duty cycle. Earlier reports on the variability characteristics of the blazar PG 1553 + 113 on intraday timescales point towards low duty cycle (Stalin *et al.* 2005; Osterman *et al.* 2006; Andruchow *et al.* 2007, 2011; Gopal-Krishna *et al.* 2011; Gupta *et al.* 2016; Zibecchi *et al.* 2017; Pasierb *et al.* 2020).

In another study by Meng *et al.* (2018), PG 1553 + 113 were performed for 28 nights in three intermediate-band filters using four statistical tests. The authors find no INV during any of the observing nights. Ours and literature data together resulted in a total of 74 intranight observations and out of which

the source was found to be genuinely variable on only eight nights (duty cycle 10.8%). This is in agreement with Andruchow *et al.* (2014) where authors reported a duty cycle of 11.6% for PG 1553 + 113. On 5 other nights, the blazar was possibly variable including which duty cycle came out to be 17.6%. Whereas, on longer timescales, the source was found to be significantly variable.

INV in blazars can be attributed to the interactions of shocks with small-scale structures, e.g., the density inhomogeneities or eddies. Therefore the strong magnetic field in HBLs (Sambruna *et al.* 1996) could explain the low DC. As the magnetic field value exceeds the critical one, the axial field halts the build-up of Kelvin–Helmholtz instabilities (Romero 1995) where the critical magnetic field is defined as:

$$\mathcal{B}_{\rm c} = [4\pi n_{\rm e} m_{\rm e} c^2 (\Gamma^2 - 1)]^{1/2} \Gamma^{-1}, \quad (1)$$

where $n_{\rm e}$ is the local electron density, $m_{\rm e}$ the rest mass of the electron and Γ the bulk Lorentz factor of the flow. Therefore, in such case, HBLs will have no instabilities thus reducing the incidence of intraday variability in their optical LCs.

We then analyzed the color-magnitude diagrams for PG 1553 + 113, viz., $B - I$, against the R magnitude (Massaro & Trèvese 1996) on diverse timescales. The flux variations were found to be achromatic for both long and short timescales, except the 2019 flare. A RWB chromatism was evident during the faint state of the source while a BWB the source is bright. Our result is similar to Ikejiri *et al.* (2011) where authors observed the source in the *VJKS*-bands from 2008 to 2010. A much denser sampling was achieved by Wierzcholska *et al.* (2015) in *BR*-bands from 2007 to 2012 when the authors reported a statistically non-significant RWB trend on a long term basis while considering both RWB and BWB behavior on shorter timescales. The characteristic spectral index of the blazar over the period from 2005 to 2019 is $\alpha = 0.89 \pm 0.06$.

The analysis of the 2019 flare shows a clockwise hysteresis loop and a soft lag, which can be attributed to the synchrotron cooling of accelerated electrons during the flare (Bessell *et al.* 1998). We fitted the flare with an exponential law (Valtaoja *et al.* 1999) plus a linear base level defined as below:

$$F(t) = \begin{cases} a + bt + \exp[+(t - t_{\rm max})/\mathcal{T}_{\rm ris}] & \text{if } t \le t_{\rm max}, \\ a + bt + \exp[-(t - t_{\rm max})/\mathcal{T}_{\rm dec}] & \text{if } t \ge t_{\rm max}, \end{cases} \quad (2)$$

where (a, b) are the parameters of the local linear base level, $t_{\rm max}$ the epoch of the flare maximum and ($\mathcal{T}_{\rm ris}, \mathcal{T}_{\rm dec}$) the flare rise and decay e-folding timescales, respectively. The flare was slightly asymmetric with the rising part being steeper. But due to poor sampling of the sub-flare around MJD $\sim$8610, we assumed 2019 flare to be symmetric which in turn implies that the cooling time is smaller than or comparable to the light crossing time. The above fit confirmed the time lag found by the DCF and ZDCF $\mathcal{T}_{\rm fit} = (2.6 \pm 0.2)$ days within the uncertainties quoted.

We addressed the periodicity of our source using the historical *VR*-band LCs with three different methods. Our analysis gives a median period of [2.21 ± 0.04 (s.d.)] years. This is similar to the findings from the previous studies of Sandrinelli *et al.* (2018) and Covino *et al.* (2020). The first hint of a (2.18 ± 0.08) years period was proposed by Ackermann *et al.* (2015) using the *Fermi*/LAT γ-ray light curve (LC) of the target. This was later conformed by various other authors at γ-rays, e.g., Prokhorov & Moraghan (2017), Tavani *et al.* (2018), Sandrinelli *et al.* (2018) and Covino *et al.* (2020) while Cutini *et al.* (2016), Sandrinelli *et al.* (2018) and Covino *et al.* (2020) confirmed the same in the *R*-band. Peñil *et al.* (2020) presented the most comprehensive QPO search at γ-rays using ten different methods along with their significance estimation. Various theoretical models, such as a binary black hole model (Valtonen *et al.* 2008; Graham *et al.* 2015), jet precession (Sandrinelli *et al.* 2016), oscillation modes of the accretion disc (Bhatta *et al.* 2016), rotating hotspots in the innermost stable orbit of the SMBH (Gupta *et al.* 2019), have been proposed to explain the multi-frequency QPOs in blazars on diverse timescales.

This hint of an year-long QPO in the blazar PG 1553 + 113 could be attributed to the jet precession in a binary system of SMBHs and/or the helical structure in the Doppler boosted relativistic jets (Caproni *et al.* 2017; Tavani *et al.* 2018). The precession causes the periodic changes in the angle between the jet axis and our line of sight, thus, the corresponding Doppler factor. The observed flux emission is related to the intrinsic one as: $F^{(\rm obs)} = \delta^{(\alpha+2)} F$. But, due to the above changes in the jet viewing angle, we have $\delta = \delta(t)$ and hence, $F = F(t)$.

In addition to the above, there is another peak above the 99% significance level at a period of (248 ± 12) days (Figure 5, a hint of this secondary period (250 ± 60 days) has also been found by Sandrinelli *et al.* (2017). Nilsson *et al.* (2018) also

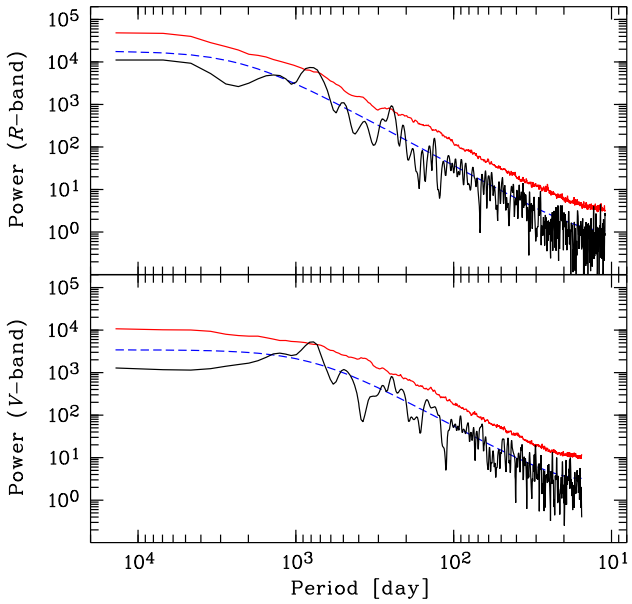

Figure 5. Output from the REDFIT programme. The black line shows the bias-corrected power spectrum, the blue dashed line marks the theoretical red noise spectrum and the red line marks the 99% local significance level derived using Monte Carlo simulations.

reported the most significant rest-frame period – 174 days which is in agreement with the above periods. To further cross-check the possible period of 200–250 days, we used the LSP method and the REDFIT. The most significant periods estimated by REDFIT are: (211 ± 10) days and (210 ± 8) days, for the *VR*-band LCs, respectively. Due to the achromaticity of the LCs, these periods could be of geometric origin such as the emitting region follows a spiral path within the jet, the jet itself has a helical geometry, or jet wobbling (Agarwal *et al.* 2015; Lico *et al.* 2020) could contribute to some extent to the periodic STV. Moreover, the observed periodicity along with the achromatic flux variation detected supports the geometric origin of the short- to long-term flux variations in PG 1553 + 113. To conclude, the issue of periodicity in blazars needs further investigation in order to confirm or reject the period. Moreover, modeling multi-frequency blazar SEDs over diverse timescales is very important to have a better understanding of blazars and dominant emission processes.

Acknowledgments

BM is supported by the Bulgarian National Science Fund of the Ministry of Education and Science under grant DN 18/13-2017. SZ acknowledges NCN grant No. 1028/29/B/ST9/01793. We thank TUBITAK National Observatory for partial support in using T60 and T100 telescopes with project numbers 1505 and 1486, respectively. AO was supported by the Scientific Research Project Coordination Unit of Ataturk University, Project ID 8418. Data from the Steward Observatory spectropolarimetric monitoring project were used. This program is supported by Fermi Guest Investigator grants NNX08AW5 6G, NNX09AU10G, NNX12AO93G and NNX15A U81G. Based on observations obtained with the Samuel Oschin 48-inch Telescope at the Palomar Observatory as part of the Zwicky Transient Facility project. ZTF is supported by the National Science Foundation under Grant No. AST-1440341 and collaboration including Caltech, IPAC, the Weizmann Institute for Science, the Oskar Klein Center at Stockholm University, the University of Maryland, the University of Washington, Deutsches Elektronen-Synchrotron and Humboldt University, Los Alamos National Laboratories, the TANGO Consortium of Taiwan, the University of Wisconsin at Milwaukee and Lawrence Berkeley National Laboratories. Operations are conducted by COO, IPAC and UW. The iPTF project is a scientific collaboration between Caltech; Los Alamos National Laboratory; the University of Wisconsin, Milwaukee; the Oskar Klein Centre in Sweden; the Weizmann Institute of Science in Israel; the TANGO Program of the University System of Taiwan; and the Kavli Institute for the Physics and Mathematics of the Universe in Japan. The CSS survey is funded by the National Aeronautics and Space Administration under Grant No. NNG05GF22G was issued through the Science Mission Directorate Near-Earth Objects Observations Program. The CRTS survey is supported by the U.S. National Science Foundation under grants AST-0909182. Based on data acquired at Complejo Astronómico El Leoncito, operated under agreement between the Consejo Nacional de Investigaciones Científicas y Técnicas de la República Argentina and the National Universities of La Plata, Córdoba and San Juan (proposals JS-2019A-10, JS-2019A-16, HSH-2018B-03 and Staff time).

References

Ackermann M., Ajello M., Albert A., *et al.* 2015, ApJL, 813, L41

Agarwal A., Gupta A. C. 2015, MNRAS, 450, 541

Agarwal A., Gupta A. C., Bachev R., *et al.* 2015, MNRAS, 451, 3882

Agarwal A., Mohan P., Gupta A. C., *et al.* 2017, MNRAS, 469, 813
Agarwal A., Cellone S. A., Andruchow I., *et al.* 2019, MNRAS, 488, 4093
Ait Benkhali F., Hofmann W., Rieger F. M., *et al.* 2020, A&A, 634, A120
Alexander T. 1997, Astronomical Time Series, 218, 163
Andruchow I., Cellone S. A., Romero G. E. 2007, Boletin de la Asociacion Argentina de Astronomia La Plata Argentina, 50, 299
Andruchow I., Combi J. A., Muñoz-Arjonilla A. J., *et al.* 2011, AAP, 531, A38
Andruchow I., Cellone S. A., Romero G. E. 2014, Revista Mexicana de Astronomia y Astrofisica Conference Series, 44, 95
Bessell M. S., Castelli F., Plez B. 1998, A&A, 333, 231
Bhatta G., Zola S., Stawarz Ł., *et al.* 2016, ApJ, 832, 47
Bhatta G., Webb J. 2018, Galaxies, 6, 2
Böttcher M., Reimer A., Sweeney K., *et al.* 2013, ApJ, 768, 54
Camenzind M., Krockenberger M. 1992, A&A, 255, 59
Caproni A., Abraham Z., Motter J. C., *et al.* 2017, ApJ, 851, L39
Cerruti M. 2020, Galaxies, 8, 72
Covino S., Sandrinelli A., Treves A. 2019, MNRAS, 482, 1270
Covino S., Landoni M., Sandrinelli A., *et al.* 2020, ApJ, 895, 122
Cutini S., Ciprini S., Stamerra A., *et al.* 2016, Active Galactic Nuclei 12: A Multi-Messenger Perspective (AGN12), 58
Drake A. J., Djorgovski S. G., Mahabal A., *et al.* 2009, ApJ, 696, 870
Edelson R. A., Krolik J. H. 1988, ApJ, 333, 646
Falomo R., Treves A. 1990, PASP, 102, 1120
Falomo R., Scarpa R., Bersanelli M. 1994, ApJS, 93, 125
Filippenko A. V., Li W. D., Treffers R. R., *et al.* 2001, IAU Colloq. 183: Small Telescope Astronomy on Global Scales, 246, 121
Gopal-Krishna, Wiita P. J. 1992, A&A, 259, 109
Gopal-Krishna, Goyal A., Joshi S., *et al.* 2011, MNRAS, 416, 101
Graham M. J., Djorgovski S. G., Stern D., *et al.* 2015, Nature, 518, 74
Green R. F., Schmidt M., Liebert J. 1986, ApJS, 61, 305
Gupta A. C., Fan J. H., Bai J. M., *et al.* 2008a, AJ, 135, 1384
Gupta A. C., Cha S.-M., Lee S., *et al.* 2008b, AJ, 136, 2359
Gupta A. C., Agarwal A., Bhagwan J., *et al.* 2016, MNRAS, 458, 1127
Gupta A. C., Tripathi A., Wiita P. J., *et al.* 2019, MNRAS, 484, 5785
Ikejiri Y., Uemura M., Sasada M., *et al.* 2011, PASJ, 63, 639
Itoh R., Nalewajko K., Fukazawa Y., *et al.* 2016, ApJ, 833, 77
Jayasinghe T., Stanek K. Z., Kochanek C. S., *et al.* 2019, MNRAS, 485, 961
Johnson S. D., Mulchaey J. S., Chen H.-W., *et al.* 2019, ApJ, 884, L31
Lico R., Liu J., Giroletti M., *et al.* 2020, A&A, 634, A87
Lomb N. R. 1976, APSS, 39, 447
Mangalam A. V., Wiita P. J. 1993, ApJ, 406, 420
Masci F. J., Laher R. R., Rusholme B., *et al.* 2019, PASP, 131, 018003
Massaro E., Trèvese D. 1996, A&A, 312, 810
Meng N., Zhang X., Wu J., *et al.* 2018, ApJS, 237, 30
Nilsson K., Lindfors E., Takalo L. O., *et al.* 2018, A&A, 620, A185
Osterman M. A., Miller H. R., Campbell A. M., *et al.* 2006, AJ, 132, 873
Pandey A., Gupta A. C., Wiita P. J., *et al.* 2019, ApJ, 871, 192
Pasierb M., Goyal A., Ostrowski M., *et al.* 2020, MNRAS, 492, 1295
Peñil P., Domínguez A., Buson S., *et al.* 2020, ApJ, 896, 134
Prokhorov D. A., Moraghan A. 2017, MNRAS, 471, 3036
Raiteri C. M., Stamerra A., Villata M., *et al.* 2015, MNRAS, 454, 353
Rau A., Kulkarni S. R., Law N. M., *et al.* 2009, PASP, 121, 1334
Romero G. E. 1995, APSS, 234, 49
Sambruna R. M., Maraschi L., Urry C. M. 1996, ApJ, 463, 444
Sandrinelli A., Covino S., Dotti M., *et al.* 2016, AJ, 151, 54
Sandrinelli A., Covino S., Treves A., *et al.* 2018, A&A, 615, A118
Smith P. D., Hughes R. E., Winer B. L., *et al.* 2009, http://arxiv.org/abs/0910.3398
Stalin C. S., Gupta A. C., Gopal-Krishna, *et al.* 2005, MNRAS, 356, 607
Takahashi T., Tashiro M., Madejski G., *et al.* 1996, ApJ, 470, L89
Takalo L. O., Nilsson K., Lindfors E., *et al.* 2008, American Institute of Physics Conference Series, 1085, 705
Tavani M., Cavaliere A., Munar-Adrover P., *et al.* 2018, ApJ, 854, 11
Urry C. M., Padovani P. 1995, PASP, 107, 803
Valtaoja E., Lähteenmäki A., Teräsranta H., *et al.* 1999, ApJS, 120, 95
Valtonen M. J., Lehto H. J., Nilsson K., *et al.* 2008, NAT, 452, 851
Wierzcholska A., Ostrowski M., Stawarz Ł., *et al.* 2015, AAP, 573, A69
Zibecchi L., Andruchow I., Cellone S. A., *et al.* 2017, MNRAS, 467, 340